Assessment of spectroscopic methods for the characterisation of DLC films deposited by PECVD

A. POUKHOVOI[a], S. SCHIPPOREIT[a], H.-W. BECKER[b], L. CALLIARI[c], V. BUCK[a*]
[a]*Universität Duisburg-Essen and CENIDE, Fakultät für Physik, Arbeitsgruppe Dünnschittechnologie, Lotharstraße 1, Duisburg D-47057, Germany*
[b]*Ruhr-Universität Bochum, Institute für Experimentalphysik III, Universitätsstraße 150, Bochum D-44801, Germany*
[c]*Center for Materials and Microsystems, Via Sommarive, 18, I-38123 Povo (Trento) Italy*

Aim of the present work is to deposit and characterize a-C:H films by a range of spectroscopic methods in order to classify them according to their structural criteria: hydrogen and sp^3 content. In order to meet this objective, the following approach was used. Carbon films within a large range of properties were synthesised by a special RF-ICP/CCP plasma source allowing to vary particle energies from a few electronvolts to keV on the one hand and chemical composition by mixing suitable precursor gases (methane, acetylene) with hydrogen on the other hand. Analytical approaches based on FTIR and Raman spectroscopy for film characterisation have been validated by consistency between them and by calibration in comparison to techniques (e.g. NRA for hydrogen and EELS for sp^3 content) known to give reliable results without calibration but limited in applicability. The results obtained provide a means to confidently classify a-C:H materials with high spatial resolution, even on "3D"-samples, without destruction of the workpiece, and thus can contribute to quality assurance in industrial coating.

(Received October 4, 2011; accepted April 11, 2012)

Keywords: PECVD, A-C:H films, ICP, CCP, spectroscopic methods, FTIR, Raman

1. Introduction

Shortly after the first successful deposition of hard amorphous carbon films the name "DLC" has been coined. Despite the advantage that this name sounds good, it has the significant disadvantage that a whole class of materials with properties ranging between diamond, graphite and polymers is covered by the same name. This hinders several applications significantly, because if the first coating failed, it might be extremely difficult to convince an automotive engineer or even an orthopaedic surgeon that another DLC may perform well, because DLC may be totally different from DLC.

First attempts to classify (homogeneous) amorphous carbon films go back about 20 years. In 1988, Angus introduced a diagram [1] where atom number density is plotted against atomic fraction hydrogen. Only three years later he modified this into a diagram where the amount of sp^3 bonds is plotted against hydrogen content [2] and worked out the "Fully constrained network" (FCN) model to explain correlations between the amount of sp^3 bonds and the hydrogen content. This scheme is used until today, but usually plotted as triangular phase diagram (see e.g. [3]). A lot of work has since then be carried out to produce films "left" from the FC regime (ta-c, ta-C:H) and Lifshitz [4] and Robertson [5,6] worked out the "subplantation model" showing the influence of energetic ions.

A solution for widespread industrial application should be based on measurement equipment that is easily accessible in usual analytical laboratories and – additionally and important for quality assurance – is non destructive and operates well on industrial "3D"-parts. Both requirements are fulfilled by spectroscopic methods.

Thus in this approach a classification that is correct from a scientific point of view (and calibrated by methods not easily accessible) is worked out for DLC-films deposited by PECVD (containing more than 20% hydrogen).

2. Experimental

2.1. Plasma source and film deposition

A disadvantage of many PECVD methods for the deposition of a-C:H films, including conventional capacitively coupled plasma, is the characteristic interdependence of plasma density and ion energy. Using a radio frequency (RF) - ICP/CCP source (inductively and capacitively coupled plasma) instead allows to precisely control ion energies and flux density of the deposited particles independently. This method produces a high plasma density of 10^{11} cm^{-3} at low pressures of 0.1-10 Pa, which are good conditions for high deposition rates. The plasma is generated by an inductive RF discharge, and the substrate, onto which the material is deposited, can be applied to a capacitively coupled bias voltage largely independently of the inductive plasma generation. The variability of the bias voltage makes it possible to selectively manipulate the energies of the ions which reach

the substrate without changing other plasma parameters. The ion energies can be set to values as low as a few eV for the plasma source described. The second important benefit of this plasma source is a homogeneous distribution of the plasma particles.

The films investigated have been deposited in a GEC reference cell (Gaseous Electronics conference [7]), which is provided with a RF ICP/CCP plasma source (13.56 MHz) (Figure 1). The bifilar flat spiral antenna design, which has been developed by Kadetov [8], allows to reduce the capacitive part of the spiral to negligible levels.

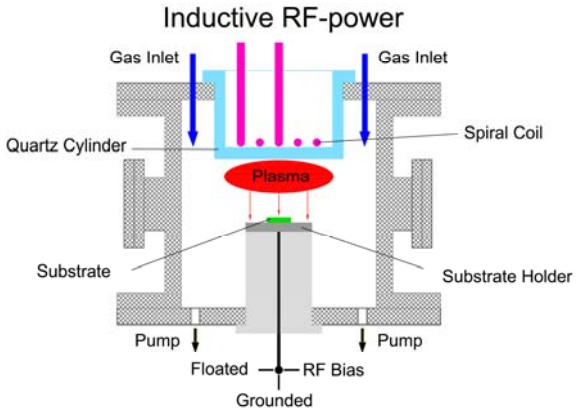

Fig. 1. GEC cell with an RF-ICP/CCP plasma source.

a-C:H films have been coated onto p-Si(111) substrates as well as onto glass (BK7) substrates . For surface purification, the substrates are treated in an ultrasonic bath for 15 minutes in acetone precursor gases for the depositions were methane (CH_4) and acetylene (C_2H_2) as well as both mixed with hydrogen (H_2). Helium has been chosen as the carrier gas. Adding heavier inert gases to the precursor gas caused increasing film stress [9], which can result in lower adhesion. Coatings made with He showed improved adhesion compared to coatings made with Ar as carrier gas.

Important coating parameters were the H/C ratio in the gas mixtures and the self-bias voltage. The process pressure was kept constantly at 10 Pa at each deposition and the ICP power was set to 100 W. The other process parameters are shown in Table 1.

Table 1. Coating parameters.

H/C	Gas flow rate, *sccm*				P_{ICP}, [*W*]	U_{bias}, [*V*]	plasma mode	time, [*min*]
	C_2H_2	CH_4	H_2	He				
1	8	-	-	50	100	0 → -200	ICP/CCP	5-60
2.375	8	-	11		100			
3.75	8	-	22		100			
4	-	8	-		-	-300 → -1200	CCP	
9.5	-	8	22		-			
16	-	4	24		-			

The coatings were made with different plasma source operating modes, which are "ICP/CCP mode" and pure "CCP mode". Plasma-enhanced deposition is characterised by competing etching and deposition processes at the surface. The balance between both processes depends on plasma density as well as the kinds and energies of the plasma species. Fig. 2 illustrates that the deposition rates of a-C:H films differ significantly for ICP/CCP and CCP discharges.

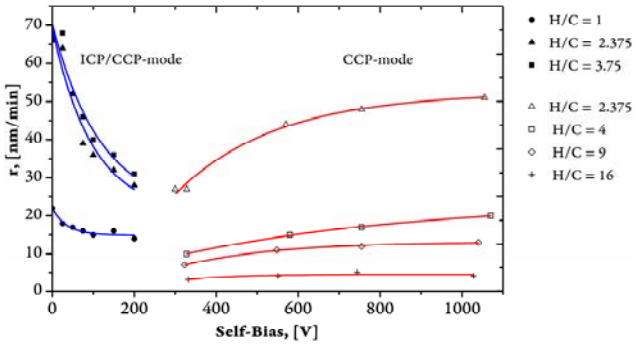

Fig. 2. Deposition rates depending on coating parameters.

A reduction of the effective film growth rate in ICP/CCP mode can be traced back to an increase of the etching rate at the film caused by atomic hydrogen. The inductively coupled plasma has a very high density and degree of gas dissociation, which results in a higher concentration of atomic hydrogen than in a CCP discharge. The higher atomic hydrogen concentration in ICP mode was confirmed by mass spectra measurements. This causes a higher gas temperature in the ICP discharge, and, thus a higher substrate temperature. Thermally induced splitting-offs of methyl end groups cause heavy erosion [10]. Etching processes are dominant when using ICP/CCP mode with methane as a precursor gas and its mixture with hydrogen ($H/C \geq 4$). This is why film growth cannot be observed. The same effect occurs when the inductively coupled power is increased. An effective film growth has been achieved with a process gas which is composed of acetylene and hydrogen ($H/C \leq 4$).

When using CCP mode, only little atomic hydrogen is formed, which results in a higher deposition ratio (H/C = 16). Thus, hydrogen ions are more likely to contribute to film growth than to film erosion. When acetylene was used as precursor gas ($H/C < 4$), little dust particles evolved due to polymerisation, which has negative effects on film quality. These volume recombinations of already dissociated carbon hydrogen radicals in acetylene plasma are described in [11].

Apparently, plasma-chemical processes are important during a-C:H film growth.

2.2. Film analysis

The measurements of the structural characterisation and hydrogen contents of amorphous carbon films were made with Raman and Fourier transform infrared spectroscopy (FTIR) respectively. The Raman spectra were measured with the micro-Raman spectrometer LabRAM (*Jobin Yvon*), which is equipped with an Ar laser with a wavelength of 514 nm and a He-Ne laser with a

wavelength of 633 nm. The FTIR measurements were done with the FTIR spectrometer EQUINOX® IFS55 (*Bruker*) in a spectral range from 7500 cm^{-1} to 370 cm^{-1} using reflection mode. An ATR (attenuated total reflectance) crystal increases the number of reflections and thus amplifies the spectra, which is important for analysing thin films. Deconvolution and spectral analysis allow conclusions to be drawn about configurations of C-H bonds, sp^3/sp^2 ratios, and H_2 contents.

Raman scattering is based on inelastic interactions between photons (excitation sources) and certain quanta of lattice vibration of solids (optical phonons). Complex bonds and structures in amorphous carbons make theoretical analysis of Raman spectra complex and in some cases ambiguous – also because data are determined mainly empirically by comparing data of different measuring methods. Furthermore, for the visible light sources used, the Raman activity of sp^3-hybridised carbon atoms is 50 – 230 times smaller than of sp^2 bond carbon [12].

A Raman spectrum of amorphous carbon is mainly characterised by its G-peak, D-peak and a photoluminescence background. In the so called G-band (1500 – 1630 cm^{-1}), there are Raman-active vibrational states of graphite (E_{2g} at 1581 cm^{-1}) and also a few pairs of sp^2-hybridised carbon atoms. A broad D-band (A_{1g} at 1360 cm^{-1}) is not identical with the band at 1332 cm^{-1}, which is due to sp^3-hybridised carbon. This sideband, the so called disorder-mode, is caused by disorder in sp^2-hybridised carbon atoms. The photoluminescence background is caused by the recombinations of the excitons within sp^2 bond clusters in a sp^3 bond amorphous matrix [13]. Hydrogen plays an important role because it saturates mainly non-emitting recombination centres.

Ferrari et al. [14] give the correlation between sp^3 content and the I_D/I_G ratio and also between the sp^3/sp^2 ratio and the G peak position of a-C:H films (Fig. 3).

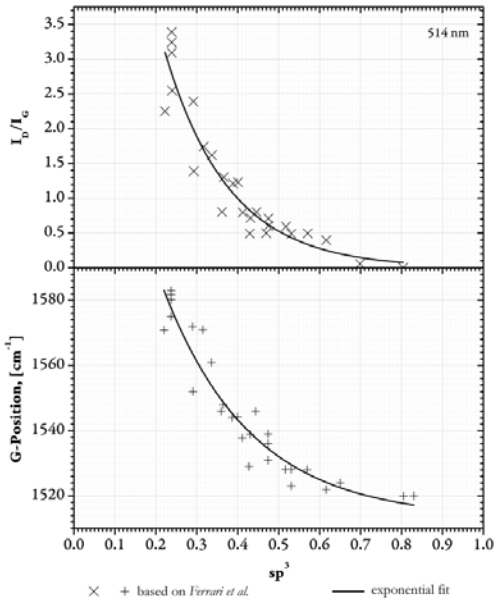

Fig. 3. Correlation between sp^3 content and parameters from Raman measurements of a:C-H films for 514 nm excitations.

A further important effect in visible Raman spectra of a-C:H films is a growing photoluminescence (PL) background with increasing hydrogen content. The ratio between the slope *m* of the fitted linear PL background and the *G* peak intensity I_G can be empirically used as a measure for the content of bonded hydrogen [15]:

$$H[at.\%] = 21.7 + 16.6 \log\left\{\frac{m}{I_G}[\mu m]\right\}. \tag{1}$$

Fourier transform infrared spectroscopy is a kind of spectroscopy which is based on the measurement of the wavelength and the intensity of mid-wave infrared light absorbed by a sample. The absorption bands in amorphous carbon are caused by CC- and CH-vibrations. Their qualitative and quantitative analyses are used for elaborating information about structures and chemical compositions of a-C:H films. In qualitative analysis, the identity of a compound, for example, is detected by a comparison of spectra. In quantitative analysis, the identification of bond configurations and of the H_2 content is done by interpretation of selected absorption bands.

A quantitative determination of the concentration of CH_x configurations has to be done carefully, because the relation of each CH configuration to the total IR absorption is different. Thus, a calibration factor B_i was used to describe the different absorption strengths of the CH vibration modes. The integral over the absorption band $A_i = \int \alpha_i(\tilde{\nu}) d\tilde{\nu}$ which belongs to a certain CH configuration is given by:

$$A_i = \int \alpha_i(\tilde{\nu}) d\tilde{\nu} = \sigma_i \cdot \tilde{\nu}_i \cdot N_i , \tag{2}$$

where α_i = differential absorption coefficient of the vibrational mode i [cm^{-1}], $\int \alpha_i(\tilde{\nu}) d\tilde{\nu}$ = integrated partial absorption coefficient of the vibrational mode i (our fit) [cm^{-2}], N_i = density of the infrared active CH_x bond [cm^{-3}], σ_i = infrared cross section of a infrared active CH_x bond [cm^2], $\tilde{\nu}_i$ = wave number of vibrational mode i [cm^{-1}]. The defined infrared cross section is given by [16]:

$$\sigma_i = \frac{\ln(10)}{\tilde{\nu}_i \cdot N_{Avo} \cdot f_i} B_i , \tag{3}$$

where B_i = calibration factor which stands for the ratio of a CH_x vibrational mode to the integrated absorption [cm^{-2} *l* mol^{-1}] (table values [16]), N_{Avo} = Avogadro constant [mol^{-1}], f_i = number of hydrogen atoms in a CH configuration: one (CH), two (CH_2), or three (CH_3). The density N_i of infrared active CH_x bonds is:

$$N_i = \frac{\int \alpha_i(\tilde{\nu}) d\tilde{\nu}}{\ln(10) \cdot B_i} N_{Avo} \cdot f_i , \tag{4}$$

with N_i, the ratio sp^3/sp^2 of infrared active bonds can be

calculated as:

$$\frac{sp^3}{sp^2} = \frac{\sum N_i(CH_x sp^3)}{\sum N_i(CH_x sp^2)}, \quad (5)$$

The hydrogen content in the film can be determined as [17]:

$$[H] = \frac{A}{(1.68 \cdot 10^5)\rho + 0.916A}, \quad (6)$$

with A = integrated total absorption [cm^{-2}] and ρ = density of the a-C:H film (g/cm³).

In addition to the spectroscopic analyses, the hydrogen contents of some selected samples were measured at with NRA, and the sp³/sp² ratios are determined by low energy EELS.

In order to measure film thicknesses, lines were drawn on substrates with a permanent marker before deposition. The material deposited on such lines can be easily removed in an ultrasonic bath. In this way, a sharp edge is produced on each substrate at which the film thickness can be measured with the mechanical *profilometer Stylus DEKTAK 6M* (*Veeco*). For determination of the density, the glass substrates were weighed before and after the film deposition.

The optical film properties and the band gap energies were analysed using UV/VIS-spectroscopy. All transmission measurements were taken with a UV/VIS/NIR-lambda 9 Spectrophotometer (*Perkin-Elmer*) for the wavelength range between 200 nm and 2500 nm. The measured spectra have been simulated with the program SCOUT 2.3 using the corresponding dielectric function.

For quantitative description of the fit model (dielectric function), two harmonic oscillators were used for intraband transitions in the conduction band, ans the OJL model (O'Leary, Johnson, Lim) for interband transitions in amorphous materials [18]. The parameters of the dielectric model function were varied until the measured and the fitted graph agreed.

3. Results and discussion

3.1. Raman spectroscopic characterisation

The Raman spectra of a-C:H films were fitted with a Gaussian function. The bond configurations in the films, peak positions, intensities, line widths, and the dependence of the G-peak on the excitation wavelength (G-dispersion) were considered for the characterisation of the films (Fig. 4).

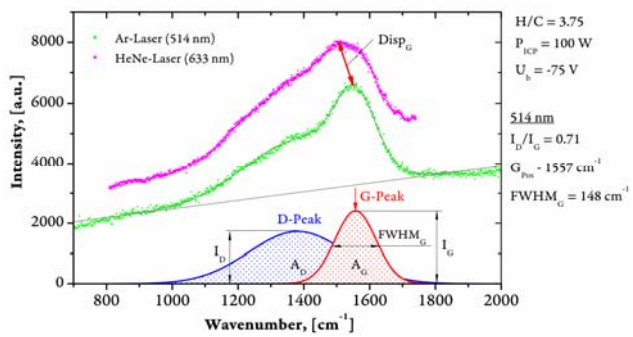

Fig. 4. Dual-wavelength Raman analysis of a-C:H.

In Fig. 5, a test series of Raman spectra is depicted. A strong photoluminescence background is clearly visible at low bias voltage (U_b = 0 – 50 V), which indicates a high hydrogen content in the films.

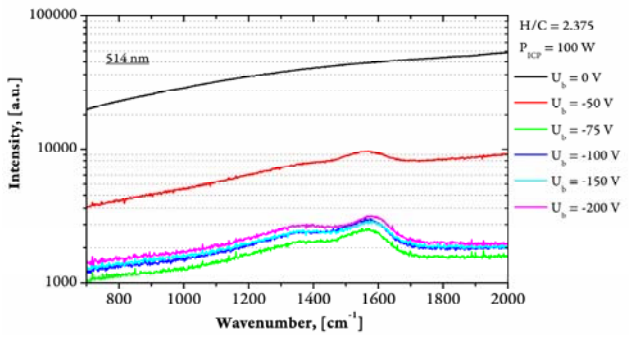

Fig. 5. Spectra of a:C-H films with H/C = 2.375.

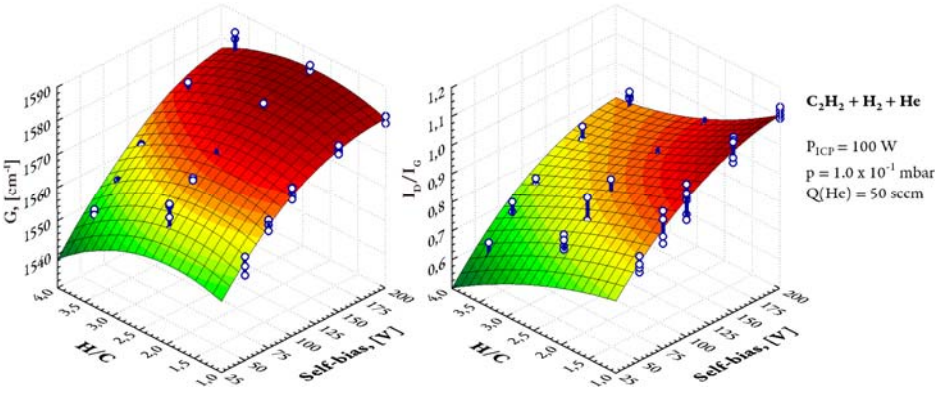

Fig. 6. Dependence of G-peak and the ID/IG ratio on coating parameters.

Fig. 6 shows the dependence of the G-peak position and of the I_D/I_G ratio on coating parameters. Apparently, the influence of the bias voltage is higher than the H/C atomic ratio in the gaseous mixture.

A higher bias voltage leads to a change of the G-peak position to a higher wave number and a higher I_D/I_G ratio. An increase of the H/C ratio leads to a decrease of the I_D/I_G ratio. The lower I_D/I_G ratio results in a higher proportion of sp^3-bonds. The G-peak vibrational states depend on the local surrounding. A change of the G-peak to lower frequencies is indicative of films with higher hydrogen contents and a higher sp^3/sp^2 ratio. In addition, the inner layer tension can lead to a change of the G-peak position. Layers with compressive stress have their G-peak at lower frequencies [19].

In amorphous carbon, the position of the G-band depends on the excitation wavelength. The dispersion is proportional to the degree of disorder in a-C:H films. At higher degrees of disorder, there is a high G-dispersion, and in more ordered structures, the G-dispersion is smaller.

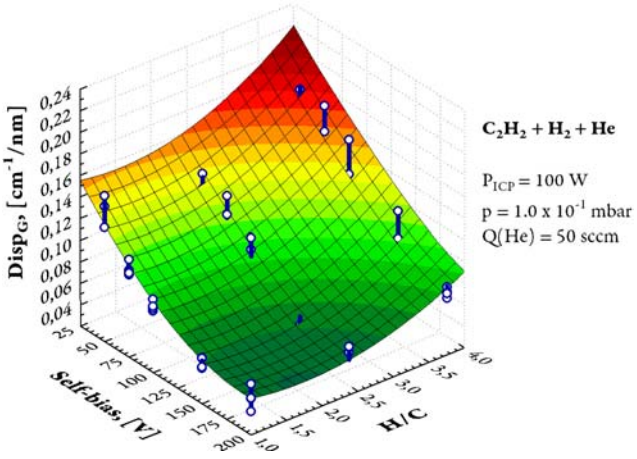

Fig. 7. Dependence of G-peak dispersion on coating parameters.

As can be seen in Fig. 7, the coating parameters influence the position of the G-peak. A small G-peak dispersion correlates with high sp^2-clustering [20]. This can be observed at high bias voltage and low H/C ratio.

The full width at half maximum (FWHM) of the G-peak is an important parameter for the estimation of the sp^2 cluster size. Its change with variation of bias voltage is shown in Fig. 8. The diagram in Fig. 9 shows sp^2 cluster sizes of 1 – 3 nm for all analysed films.

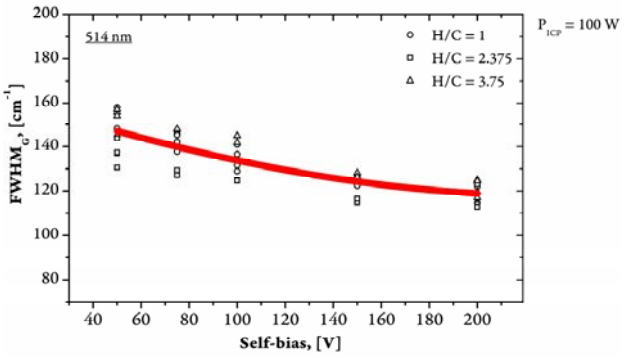

Fig. 8. Dependence of full width at half maximum (FWHM) G-peak on the bias voltage.

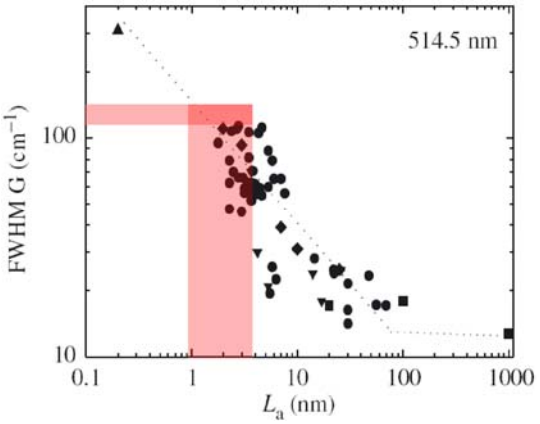

Fig. 9. Variation of the full width at half maximum of the G-peak with decreasing sp^2 cluster size L_a (at the visible excitation wavelength 514.5 nm) according to [21].

3.2. FTIR characterisation

In Fig. 10, the absorption curve of a-C:H films with H/C = 3.75 is shown. For reasons of clarity, the spectra are arranged from bottom to top with increasing bias voltage. These spectra have a good resolution and a good signal-to-noise ratio. The C-H bending vibrations are to be found between 1300 and 1500 cm^{-1}, and the C-H stretching vibrations between 2800 and 3100 cm^{-1}.

The films which were deposited without bias voltage have polymer-like structures. The vibrational bands are narrow and have a good resolution. Water can diffuse through the material along the columnar structures [16]. This is also indicated by the broad characteristic absorption bands of H_2O around 1700 and 3250 cm^{-1}. Starting with 50 V, the bias voltage causes radical changes in band structure. The absorption bands get shaped differently and get weaker and broader. Instead of water incorporation, one can now see a broad absorption band of C=C double bonds at approximately 1600 cm^{-1}.

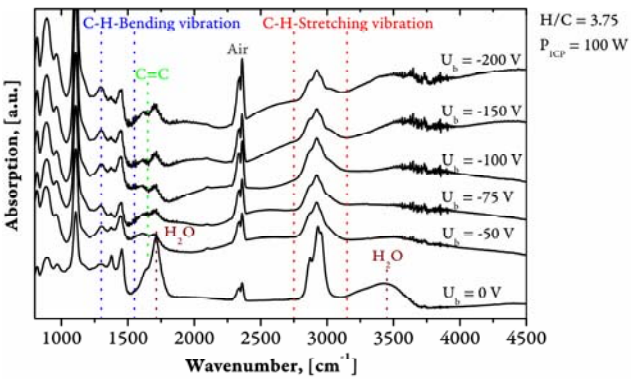

Fig. 10. Absorption spectra of a-C:H films with different self bias voltages (H/C = 3.75).

The C-H stretching vibration band was used for quantitative analyses, because it is more distinct than the C-H bending vibration band. The C-H stretching vibration band consists of vibrations of various CH_x configurations. In order to identify the parts of individual bonds, peak deconvolution was performed (Fig. 11).

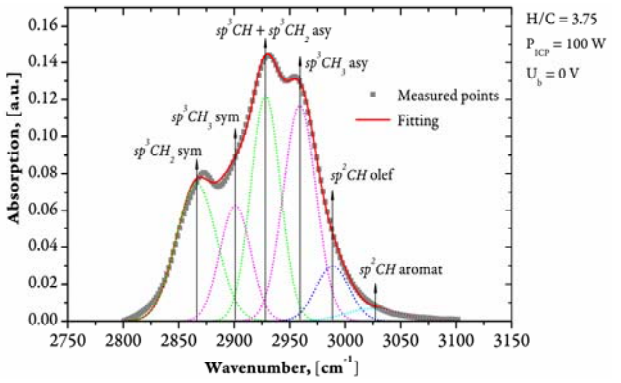

Fig. 11. Peak deconvolution of the C-H stretching vibration band of a 0 V sample.

For the deconvolution of the measured spectra, a Gaussian distribution was used for the shape of the absorption lines. Ristein et al. [16] have given a comprehensive overview of possible frequencies of the relevant vibration modes in a-C:H films. The ascription to the individual peaks were taken over with slight correction and kept constant for almost all samples (Fig. 12). The program ORIGIN 7.5 was used for deconvolution.

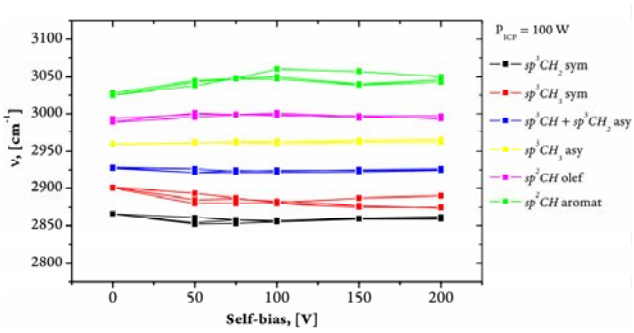

Fig. 12. Peak positions of C-H stretching vibrations.

The following kinds of stretching vibrations were found in all samples: sp^3CH, sp^3CH_2 (symmetric as well as asymmetric), sp^3CH_3 (symmetric as well as asymmetric), aromatic sp^2CH and olefinic sp^2CH. The asymmetric modes usually cause a bigger change of the dipole moment than the symmetric modes and they are more intense.

The sp^3CH stretching vibration cannot be fitted as a distinct line, because it is superposed by the more intensive asymmetric sp^3CH_2. However, one can estimate its value with an indirect method [16], assuming that the concentration of sp^3CH groups is low in polymer-like materials (bias voltage 0 V). The intensity ratio between the asymmetric sp^3CH_2 mode and a symmetric mode of 0 V-samples is 1.63, which is in accord with literature values of polymers [16]. Assuming that the intensity ratio of asymmetric sp^3CH_2 and symmetric sp^3CH_2 is equal for samples of different hardness values, the values above 1.63 can be attributed to sp^3CH. The ratios of the integrated absorption between asymmetric and symmetric modes which were used for the fits, were adopted from [16]. These ratios were 2 for sp^3CH_3 and 1.5 for sp^3CH_2. sp^3CH_3 stretching vibrations were found in each sample.

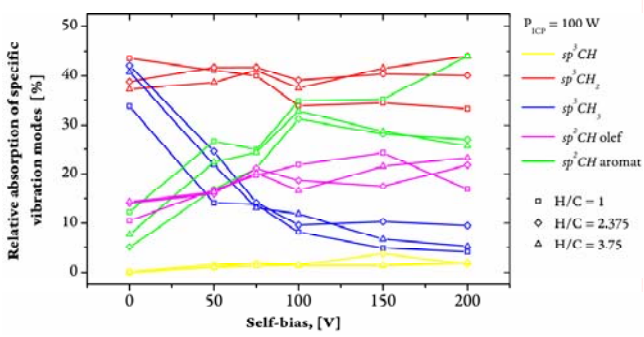

Fig. 13. Trends of the relative proportions between specific vibration modes and the total absorption of stretching vibrations as a function of bias voltage.

The relative proportions between specific CH_x vibration modes and the total absorption (N_i in %) provide information about changes in stretching vibration modes. Fig. 13 shows considerable differences between the films. A significant quantity of sp^3CH_3 vibrations could be proved in polymer-like a:C-H films. Although these methyl groups increase the proportion of sp^3 bond carbon atoms, they do not lead to extensive cross-linkage, because hydrogen atoms can only have one bond partner. This is why the chain structures are only slightly cross-linked. With increasing bias voltage and, thus, higher ion energies, the density of sp^3CH_3 bonds gets drastically reduced and the vibrations of sp^3CH bonds come up. This indicates the transition from polymeric to hard a-C:H films.

Thereby, the bond configurations change from disordered, olefinic sp^2CH to the more ordered, aromatic sp^2CH. Further increase of ion energies (above ca. 150-180 eV) leads to increasing density of sp^2CH bonds, which is a sign of graphitisation.

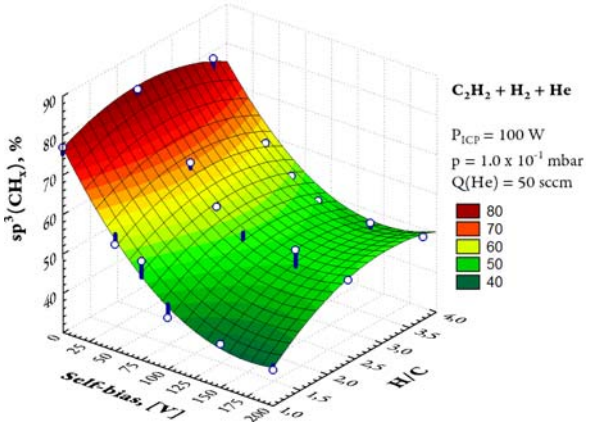

Fig. 14. Dependence of the $sp^3(CH_x)$ proportion of infrared active bonds on the coating parameters.

The sp^3 content of infrared active C-H bonds is shown in Fig. 14. The sp^3 content increases with decreasing bias voltage and increasing H/C ratio. This is in accord with the findings of Raman analysis.

Fig. 15 shows the hydrogen content calculated from FTIR spectra.

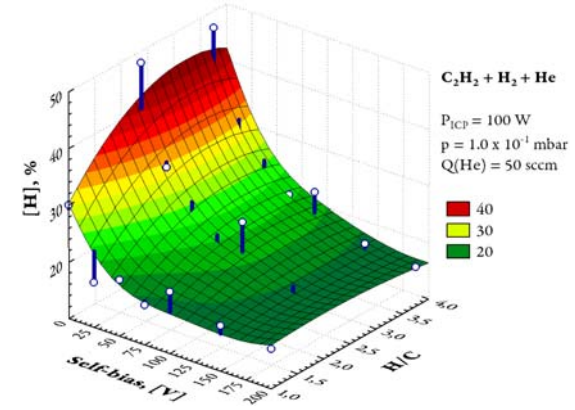

Fig. 15. Dependence of the hydrogen content on coating parameters.

Selected samples were analysed with NRA to measure the total hydrogen content. An exemplary measurement result is shown in Fig. 16. The a-C:H films have homogeneous hydrogen concentrations throughout their thicknesses. Fig. 17 shows a comparison of the hydrogen concentrations analysed via NRA and FTIR analyses. NRA analysis gives higher values than FTIR, with a maximum difference of 10%. This can be explained with the fact that FTIR measurements include only bonded hydrogen. Molecular hydrogen is not infrared active and, thus, cannot be detected with FTIR.

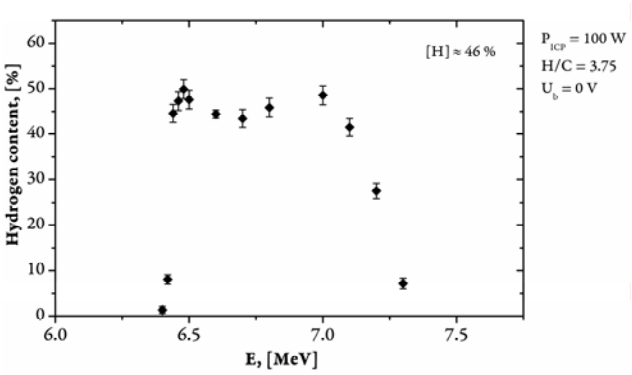

Fig. 16. NRA hydrogen profile of an a-C:H film.

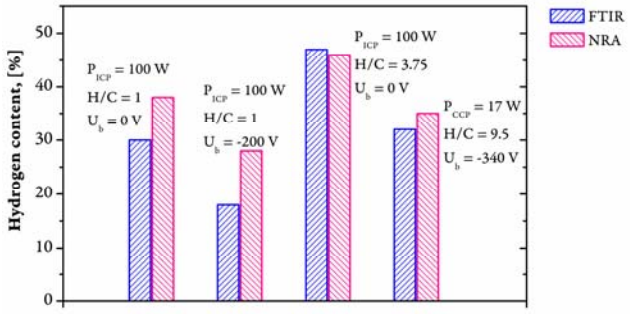

Fig. 17. Hydrogen concentrations measured with FTIR and NRA.

3.3. Characterisation of the films with UV-VIS spectroscopy

The optical spectra which were simulated with the fit model [18], assort well with the measured spectra (Fig. 18).

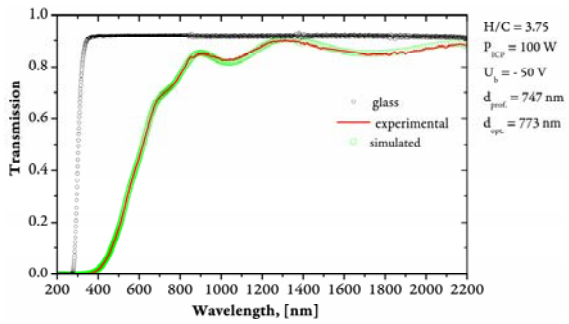

Fig. 18. Measured and simulated spectrum of an a-C:H film.

Necessary parameters such as film thickness d, band gap E_g, as well as optical constants (refractive index $n(\lambda)$, extinction coefficient $k(\lambda)$) were extracted from the simulated fit parameters. The calculated film thickness agrees with the film thickness measured with the profilometer. The deviation is less than 4%. Thus, one can conclude that this fit model is suitable for such films.

With the help of UV-VIS spectroscopy simulations, the refractive index n and the extinction coefficient k were calculated for the wave length λ = 632,8 nm. Fig. 19 shows these parameters depending on the coating parameters in two 3-D diagrams.

The bias voltage U_b has a greater impact on the optical properties than the H/C atomic ratio of the gaseous mixture used. A combined "ICP/CCP mode" produces lower refractive indexes and extinction coefficients ($1.55 \leq n \leq 2$; $0.001 \leq k \leq 0.19$) than the pure "CCP mode" ($1.85 \leq n \leq 2.35$; $0.075 \leq k \leq 0.25$).

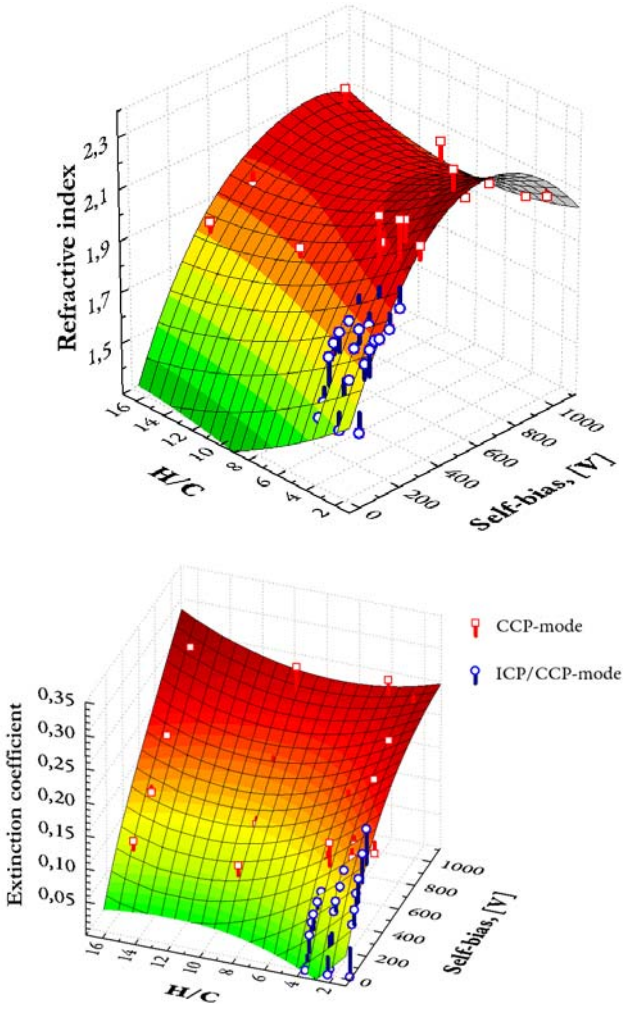

Fig. 19. Dependence of the refractive index and the extinction coefficient of a-C:H films on the coating parameters.

Fig. 20 is a 3-D diagram of the calculated band gap energy in dependence on the coating parameters. Taking into account the results of FTIR and Raman spectroscopy, suggests that the change in band gap energy is due to structural differences of the amorphous hydrocarbon films. Increasing numbers of aromatic clusters in the film, and a change from polymer-like to diamond-like material lead to a reduction of the optical band gap.

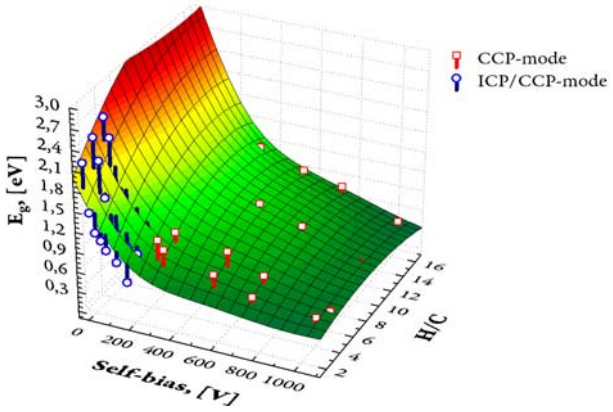

Fig. 20. Dependence of the band gap energy of a-C:H films on the coating parameters.

Fig. 21 shows the hydrogen content depending on the coating parameters calculated with equation (1). As expected, hydrogen-rich films (up to 60%) are generated at low bias voltages. With increasing bias voltage, the hydrogen content decreases, and from U_B = -75 V it remains virtually constant at approximately 35%.

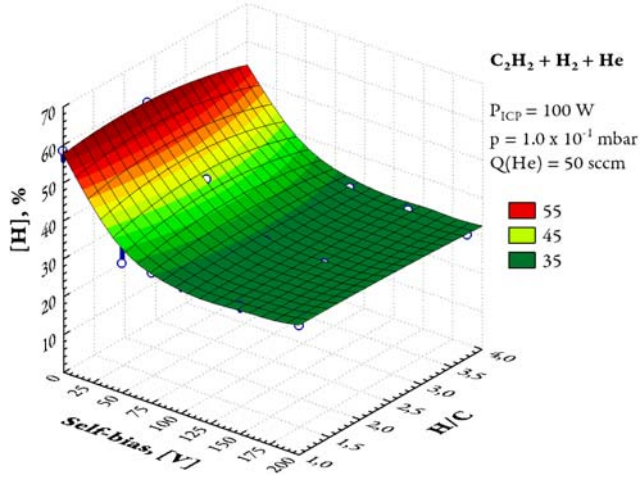

Fig. 21. Hydrogen content depending on coating parameters.

From these curves, the sp^3 content is determined using the correlation diagrams (Fig. 3) and is shown in Fig. 22. It appears that the results of both methods are different.

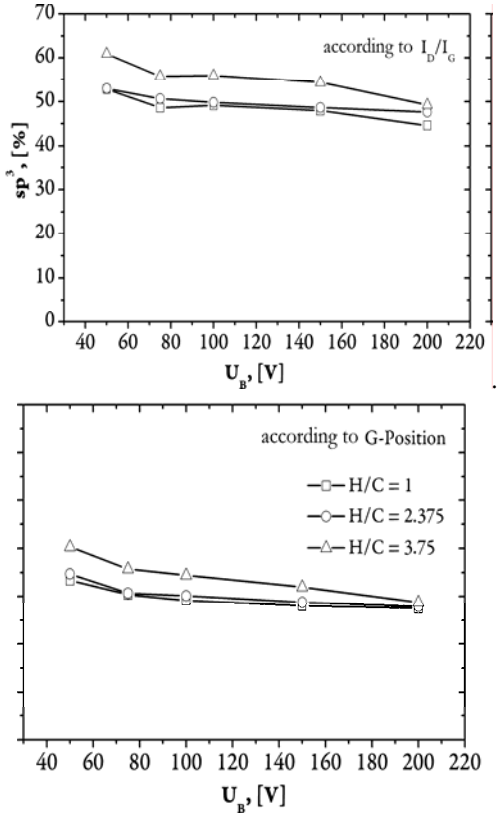

Fig. 22 determination of sp³ content from Raman measurements with I_D/I_G and the G peak position.

3.4. Comparison of the spectroscopic methods

Fig. 23 shows the sp³ content calculated from Raman and FTIR measurements depending on coating parameters.

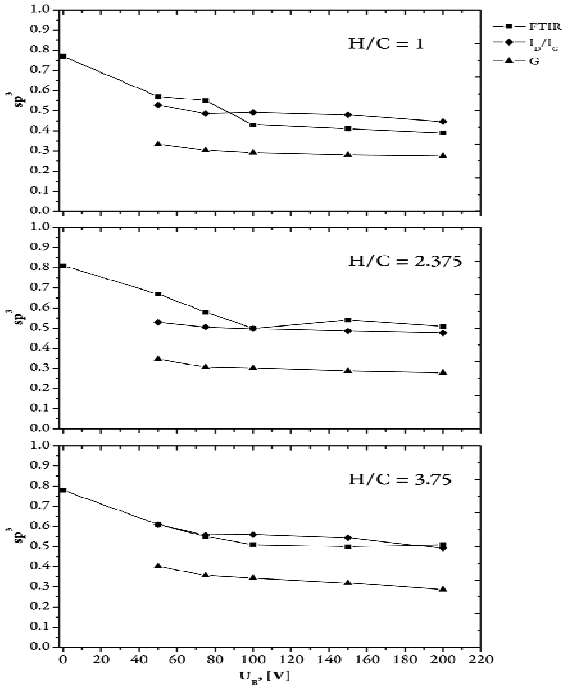

Fig. 23. Comparison of the sp³ content from Raman and FTIR measurements.

The results of FTIR analysis and from I_D/I_G of Raman spectroscopy are in accordance with each other while the values based on the G peak position are much lower.

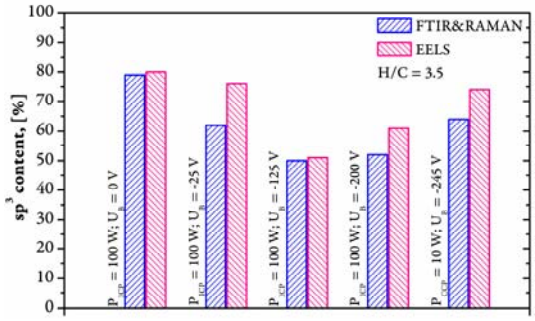

Fig 24. Comparison of sp^3 contents calculated from FTIR & Raman and from EELS measurements.

For evaluation of the spectroscopic measurements, the sp³ contents of selected samples were also determined using EELS [22]. Fig 24 shows a comparison of the sp³ content measured with Raman and FTIR (average) and with EELS. For the film with U_b = 0, the Raman measurement is not included, because of the strong luminescence background (see Fig 5). EELS provides slightly higher values, but on the whole the results of FTIR and Raman do not differ more than 15% from EELS measurements, which is acceptable for most industrial applications.

EELS values are higher because all C-bonds (carbon-hydrogen as well as carbon-carbon-hydrogen bonds) are considered when measuring sp³ contents, whereas FTIR measurements considers only carbon-hydrogen bonds. The results of FTIR measurements coincide with EELS measurements for the polymer-like film (U_b = 0), because such films do not contain virtually any non-hydride structures.

Fig. 25 shows the measured hydrogen content based on FTIR, NRA and Raman measurements.

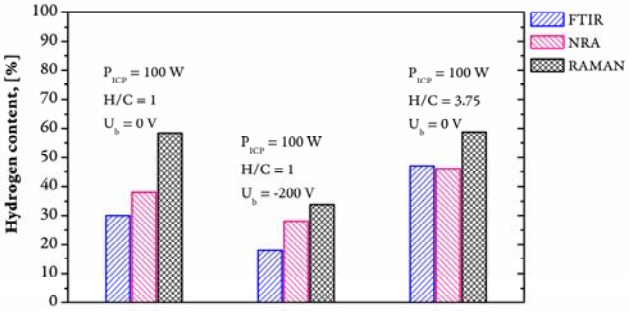

Fig. 25. Comparison of hydrogen content from FTIR, NRA and Raman measurements.

4. Conclusions

One can conclude that the hydrogen content of a-C:H

films can be determined with acceptable deviation by deconvolution of FTIR spectra as well as from Raman spectra. Raman spectroscopy gives the highest values, which can be explained by impurities which contribute the photoluminescence background. In contrast, FTIR spectroscopy normally gives the lowest values as it considers hydrogen which is bond to carbon only.

Fig. 26 shows that in ICP-CCP mode films can be produced which are "to the left" of the FCN area.

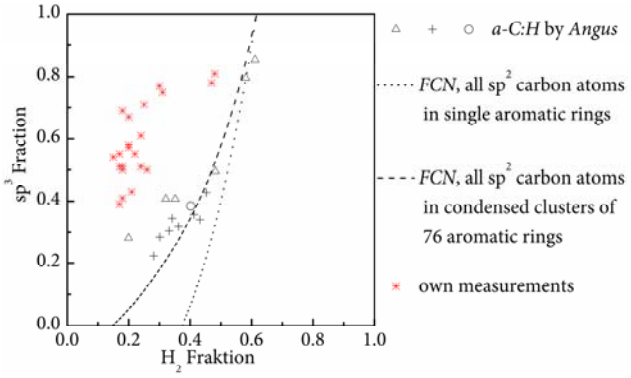

Fig 26. Deposited a:C-H films in Angus' FCN model [2].

The hybrid plasma source can produce films which are in the area between the *Y* axis (films without hydrogen) and the FCN line. Thereby, an ICP/CCP-hybrid can produce films in an exceptionally large area in the "phase diagram sp^2 / sp^3 / H", from polymer-like to ta:C-H.

It was shown that in the same area in the FCN diagram the characterization of sp^3 content as well as hydrogen content is feasible with spectroscopic methods.

References

[1] J. C. Angus, C. C. Hayman, Science **241**, 913 (1988)
[2] J. C. Angus, Diamond Relat. Mater. **1**, 61 (1991)
[3] W. Möller, Appl. Phys. **A56**, 527 (1993)
[4] Y. Lifshitz, PRL **62**, 1290 (1989)
[5] J. Robertson, Diamond Relat. Mater. **1**, 397 (1991)
[6] J. Robertson, Surf. Coatings Techn. **50**, 185 (1992)
[7] P.J.Jr. Harigs, K.E. Greenberg, P.A. Miller, J.B. Gerardo, J.R. Torczynski, M.E. Riley, G.A. Hebner, J.R. Roberts, J.K. Olthoff, J.R. Whetstone, R.J. Van Brunt, M.A. Sobolewski, H.M. Anderson, M.P. Splichali, J.L. Mock, P. Bletzinger and A. Garscadden, R.A. Gottscho, G. Selwin, M. Dalvie and J.E. Heidenreich, J.W. Butterbaugh, M.L. Brake, M.L. Passow, J. Pender and A. Lujan, M.E. Elta, D.B. Graves, H.H. Sawin, M.J. Kushner, J.T. Verdeyen, R. Horwath, and T.R. Turner, Rev. Sci. Instrum. **65**, 140 (1994).
[8] V.A. Kadetov, PhD thesis, Bochum (2004).
[9] Z. Sun, C.H. Lin, Y.L. Lee, J.R. Shi, B.K. Tay, Thin Solid Films **377-378**, 198 (2000).
[10] W. Jacob, Thin Solid Films **326**, 1 (1998).
[11] S. Stoykov, C. Eggs, U. Kortshagen, J. Phys. D: Appl. Phys. **34**, 2160 (2001).
[12] A.C. Ferrari and J. Robertson, Phys. Rev. **B61**, 14095 (2000).
[13] B. Marchon, J. Gui, K. Grannen, G.C. Rauch, J.W. Ager III, S.R.P. Silva, J. Robertson, IEEE Trans. Mag. **33**, 3148 (1997).
[14] A.C. Ferrari, J. Robertson Phys. Rev. **B61**, 14095 (2000).
[15] C. Casiraghi, A.C. Ferrari, J. Robertson, Phys. Rev. **B72**, 085401-1 (2005).
[16] J. Ristein, R.T. Stief, L. Ley, W. Beyer, J. Appl. Phys. **84**, 3836 (1998).
[17] P. Couderc, Y. Catherine, Thin Solid Films **146**, 93 (1987).
[18] S.K. O'Leary, S.R. Johnson, P.K. Lim, J. Appl. Phys. **82**, 3334 (1997).
[19] Q. Wie, R.J. Narayan, A.K. Sharma, J. Sankar, J. Narayan, J. Vac. Sci. Technol. **A17**, 3406 (1999).
[20] A.C. Ferrari, J. Robertson, Phys. Rev. **B64**, 075414 (2001).
[21] A.C. Ferrari, S.E Rodil, J. Robertson, Phys. Rev. **B67**, 155306 (2003).
[22] L. Calliari, S. Franchenko, M. Filippi, Surf. Interface Anal. **42**, 1066 (2010).

* Corresponding author: volker.buck@uni-due.de